

Experimental evidence of absolute band gaps in phononic crystal pipes

Jules Plisson, Adrien Pelat, François Gautier, Vicente Romero Garcia, Thierry Bourdon

▶ **To cite this version:**

Jules Plisson, Adrien Pelat, François Gautier, Vicente Romero Garcia, Thierry Bourdon. Experimental evidence of absolute band gaps in phononic crystal pipes. Applied Physics Letters, 2020, 116 (20), pp.201902. 10.1063/5.0007532 . hal-02613369

HAL Id: hal-02613369
https://hal.science/hal-02613369

Submitted on 20 May 2020

HAL is a multi-disciplinary open access archive for the deposit and dissemination of scientific research documents, whether they are published or not. The documents may come from teaching and research institutions in France or abroad, or from public or private research centers.

L'archive ouverte pluridisciplinaire **HAL**, est destinée au dépôt et à la diffusion de documents scientifiques de niveau recherche, publiés ou non, émanant des établissements d'enseignement et de recherche français ou étrangers, des laboratoires publics ou privés.

Experimental evidence of absolute band gaps in phononic crystal pipes

Jules Plisson,[1, a)] Adrien Pelat,[1] François Gautier,[1] Vicente Romero Garcia,[1] and Thierry Bourdon[2]
[1)]*Laboratoire d'Acoustique de l'Université du Mans, CNRS, Av. O. Messaien 72085, Le Mans, France*
[2)]*Vitesco Technologies France SAS, 44 Av. du General de Croutte, 31036, Toulouse, France*

(Dated: 20th May 2020)

The vibration filtering properties of a phononic crystal pipe whose unit cell consists of two segments of different material and cross-section are studied numerically and experimentally. Such an architected bi-material pipe leads to an alignment of the dispersion branches in the same frequency ranges for all types of waves (flexural, longitudinal, torsional), leading to an absolute band gap. Each motion is studied by a 1D model in which the propagation of Floquet-Bloch waves in lossy media are considered. The numerical optimization is based on the simplex algorithm and aims to control both the central frequency and the band width of the absolute band gap on a selected target. Experimental characterization of a demonstrator confirms the filtering effects due to partial and absolute band gaps even in the presence of quite high structural damping.

The mitigation of noise pollution is a major societal challenge for which extensive research has been conducted[1] and NVH (Noise, Vibration and Harshness) departments have been widely integrated notably in transportation industry. Structure borne sound results from bending vibrations and their couplings with other types of waves, due to the complex geometries classically encountered in industrial systems[2]. An effective reduction in the radiated sound levels then requires to mitigate all types of waves. In this context, the approach presented here concerns the design of "total filters" that can be inserted into engine components acting as structural waveguides that transmit vibrations to other components able to radiate sound. To reach such "total filter" features, the design strategy is based on the concept of absolute band gap.

The control of elastic waves by periodic structures have been dramatically developed during the last decades by using Phononic Crystals (PC)[3,4] as analogously done for light waves by Photonic crystals[5]. These systems, made of either periodic distributions of scatterers embedded in a physically dissimilar host material or simply periodic geometries, are driven by a particular dispersion relation showing band gaps[6,7], ranges of frequencies produced by the Bragg interferences in which the propagation of waves is forbidden[8]. Significant progress has been made on the control of flexural or longitudinal waves by PCs showing different applications including filtering[9,10], wave trapping[11,12], wave-guiding[13], focusing by refracting[14,15] or scattering[16] waves as well as self-collimation[17,18], among others[4]. One of the main challenges of PCs has been the design of absolute band gaps over which the propagation of all elastic waves is forbidden, whatever their polarisation and wave vector.

PCs with a fluid-type host medium, known as sonic crystals[9], have theoretically and experimentally reported absolute band gaps in broad ranges of frequencies[10,19,20]. These systems represent the most simple PC as only longitudinal waves are propagating in the medium. Perhaps the most known application of sonic crystals is the design of tunable sound screens[21–23]. However, once the host medium is a solid, the problem becomes more complex as different polarisations can be excited in the system. In this case, theoretical evidences of absolute band gaps are also widely reported in the literature. 1D PCs exhibiting absolute band gaps have been analysed by the transfer matrix method[24] and recently, 1D PCs with alternating materials in the radial and axial directions have been used to show absolute band gaps[25]. Two dimensional (2D) PC slabs consisting of either solid[26] or piezoelectric[27] inclusions placed periodically in an isotropic host material have been theoretically analysed showing absolute band gaps with a variable bandwidth for elastic waves of any polarisation and incidence. Bulk 2D PCs have been also proposed for bulk wave attenuation with solid[28] or magnetostrictive[29] inclusions. Using specialised genetic algorithms, 2D PC formed from silicon and solid voids have been optimized to obtain unit cell designs exhibiting absolute band gaps for both in- and out-of-plane motions[30].

From the experimental point of view absolute band gaps have been also reported in the literature. 2D binary solid/solid composite media with cylindrical inclusions embedded in an epoxy resin matrix showed dips of transmission evidencing the presence of absolute band gaps[31]. More recently, the presence of absolute band gaps in pillared PC slabs have been shown by double-vibrator three-components[32] and temperature-driven adaptive systems[33]. 3D PCs made of face centered cubic unit cells composed of a single material have been used to experimentally show ultra-wide absolute band gaps[34,35]. Recently, 3D load-bearing architected lattice, composed of a single material, have been designed for presenting broadband frequency band gaps for all directions and polarizations for airborne sound and elastic vibrations simultaneously[36]. However, although 2D and 3D PCs have been widely validated experimentally, less attention has been paid to the experimental analysis of 1D case acting simultaneously on longitudinal, flexural and torsional waves. The control of vibrations in such a 1D PCs systems can impact the design of piping systems which can be exploited in areas such as the automotive industry, heat exchanger tubes in chemical plants, oil pipelines, marine risers, pump discharge lines, among others[37].

In this work, we apply the concept of absolute band gap

[a)]Electronic mail: jules.plisson.etu@univ-lemans.fr;
Also atVitesco Technologies France SAS

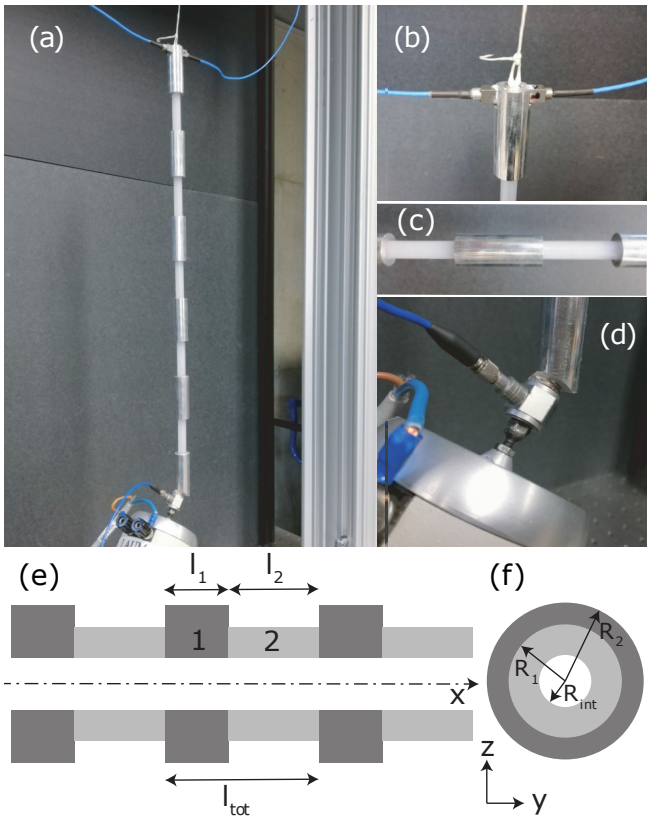


Figure 1. Scheme and pictures of the manufactured PC pipe. Nylon and aluminium sections are nested by force fitting, which holds the assembly together without the use of glue and therefore minimises unwanted losses. (a) Experimental setup; (b) Detail of the 2 face-to-face three-axis accelerometers; (c) view of the 2 aluminium/nylon unit cells of the demonstrator; (d) view of the shaker excitation implemented in the oblique position such that all wave types are excited. (e) and (f) show lateral and cross sectional schematic representation of the modeled PC pipe, respectively.

in order to design and experimentally validate 1D PCs pipes able to mitigate longitudinal, flexural and torsional waves in a same target band. A 1D PC pipe made of a unit cell consisting of two different hollow cylinders made of aluminium and nylon (see Fig.1) is optimised. Considering lossy constitutive materials, the eigenvalue problems of the three types of waves are analytically solved by imposing continuity conditions between the different parts of the unit cell and Floquet-Bloch periodic conditions at its extremities. The three problems are combined via a minimizing algorithm in order to reach the geometry of the 1D PC pipe that exhibits an absolute band gap of target central frequency and band width. Full 3D finite element simulations and experimental caracterization of a demonstrator of finite size are in good agreement and show deeps in the transfer functions associated with the predicted absolute band gap.

Figure 1(a-d) show the pictures of the 1D bi-material PC pipe used in the experiments. A detailed scheme with the geometrical parameters of the system is shown in Fig.1(e-f). Each segment of the unit cell is assumed to be a thin-walled pipe of annular cross-section. We define $\gamma = l_2/l_{tot}$ as the length ratio and $\beta = R_2/R_1$ as the outer radius ratio. The inner radius R_{int} is constant for the two segments of the unit cell. These two geometrical parameters will be used to describe the geometry in the optimisation procedure. The 1D PC pipe is made of aluminium and nylon, considered as linear and isotropic elastic materials. The nylon is characterized by its Young modulus $E_N = 2.3$ GPa, its density $\rho_N = 1240$ kg/m^3 and its Poisson ratio $\nu_N = 0.3$. The aluminium characteristics are $E_A = 71$ GPa, $\rho_A = 2170$ kg/m^3 and $\nu_A = 0.3$.

Here we consider harmonic wave motion with the time convention $e^{\imath\omega t}$. In what follows the subindex $i = N,A$ and the superindex $w = l,t$ will represent each segment of the unit cell and the wave type (longitudinal, l, or torsional, t), respectively. On the one hand, the propagation of longitudinal and torsional waves in the i-th part of the unit cell is modeled by a 1D Helmholtz equation[38]

$$\frac{\partial^2 u_i^w}{\partial x^2} + (k_i^w)^2 u_i^w = 0, \tag{1}$$

where u_i^w is the displacement of the wave w of the i-th segment of the unit cell. $k_i^w = \frac{\omega}{c_i^w}$ is the wave number with $c_i^w = \sqrt{E_i^w/\rho_i}$ the speed of the wave and $E_i^l = E_i$ is the Young modulus and $E_i^t \equiv G_i = E_i/2(1+\nu_i)$ is the shear modulus.

On the other hand, flexural waves are described using the Timoshenko's beam theory[39,40] that takes into account shear deformation and rotational inertia effects. Even this framework is based on low frequency assumptions, it makes it possible to analyse the propagation at higher frequencies or for thicker beams than with the Euler-Bernoulli's theory. Following Timoshenko assumption, the flexural displacement v_i satisfies the motion equation

$$\frac{E_i}{\rho_i}\frac{\partial^4 v_i}{\partial x^4} + \omega^2\left(1 + \frac{E_i}{\kappa_i G_i}\right)\frac{\partial^2 v_i}{\partial x^2} + \left(\frac{S_i\omega^2}{I_i} - \frac{\rho_i I_i \omega^4}{\kappa_i G_i}\right) v_i = 0, \tag{2}$$

where κ_i, S_i, and I_i are the shear coefficient, the cross-section area and quadratic moment, respectively. In order to obtain the eigenvalue problem whose solutions give the complex dispersion relation, $k_b = k(\omega) l_{tot}/\pi$, we apply the continuity boundary conditions at the interfaces between each segment of the unit cell as well as the Floquet-Bloch periodic conditions at its extremities (see Supplementary materials for more details). The resulting set of equations leads to a linear system $M(\omega, k_b).\mathbf{B} = \mathbf{0}$ where for each given ω of a frequency range of interest, the values of k_b satisfying det(M)=0 are found numerically to provide the dispersion relation. By solving each 1D model this way, we obtain the dispersion relations for all types of waves in the PC pipe. Solutions obtained by the previous semi-analytical methodology are compared to reference solutions provided by 3D elasticity finite element simulations (solid mechanics COMSOL package).

Figure 2(a) shows the real part of the dispersion relation for a PC pipe with the following geometry: $l_{tot} = 0.1$ m, $\gamma = 0.2$,

$R_1 = 8$ mm and $\beta = 0.5$. Coloured dots (each colour a wave type) represent the results obtained from the semi-analytical model while gray circles represent the FEM reference solutions. Results are in very good agreement and so the semi-analytical modeling is well validated. However, some disagreements appear for flexural waves at high frequencies (dispersion branch just under 20kHz) due to the expected limitations of the Timoshenko's beam model. Anyway, the dispersion relation obtained for this geometrical layout exhibit a wide absolute band gap in the range [3-10]kHz.

Figure 2(b) shows the evolution of the band gaps as β changes. Each coloured patch in the plot encloses the frequencies between the lower and the upper edge of the band gap. Results indicate that β essentially controls band gaps bandwidth and has a relatively weaker effect on their central frequencies. Such tendancy has already been observed in the case of monolitic corrugated beams[41].

Analogously, Fig.2(b) shows the evolution of the band gaps as γ changes. Both the central frequency and width display non monotonous variations of the same range. In particular, some optimal band widths appear around $\gamma = 0.2$. Finally γ has a more complex effect on the band gap features that do not follow any clearly identifiable law. Anyway, there are some configurations for which all band gaps overlap creating an absolute band gap. This feature is obtained in the range $[4-10]$ kHz for $\gamma = 0.2$, for example. In this case, the second flexural band gap and the first longitudinal and torsional band gaps are involved. However, Fig.2(b,c) show that it is difficult to tune by hand the absolute band gap to a target band. In order to achieve this goal, a numerical optimization procedure is proposed below.

A Nelder-Mead local minimisation algorithm[42] is used in this work to provide the geometrical parameters of a PC pipe with an absolute band gap defined from both a target central frequency f_0 and a target band width Δf_0. The set of parameters subject to the optimisation is defined as $X = [l_{tot}, \gamma, R_1, \beta]$. It is worth noting here that the first unit cell segment will be made of aluminium and the second one of nylon. The cost function $\mathscr{F}$ is defined as a weighted sum of two convergence indicators and reads

$$\mathscr{F} = \alpha_{f_c} I_{fc} + \alpha_{\Delta f} I_{\Delta f}. \tag{3}$$

The weighting coefficients α_{f_c} and $\alpha_{\Delta f}$ are adjustable such that $\alpha_{f_c} + \alpha_{\Delta f} = 1$ and the convergence indicators are defined by

$$I_{\Delta f} = \left| 1 - \frac{\Delta f - \Delta f_0}{\Delta f + \Delta f_0} \right|, \tag{4}$$

$$I_{fc} = \left| 1 - \frac{f_c - f_0}{f_c + f_0} \right|, \tag{5}$$

with Δf=min$\left(f_{max}^{(i)}\right)$-max$\left(f_{min}^{(i)}\right)$ the absolute band width and $f_c = \frac{1}{2}\left[\max\left(f_{min}^{(i)}\right) + \min\left(f_{max}^{(i)}\right)\right]$ the central frequency. $f_{max,min}^{(i)}$ represents the upper (index *max*) and lower (index *min*) edges of the band gap for the i-th wave where the subindex i represents each type of wave type $i = F, L, T$ for flexural, longitudinal and torsional waves respectively. I_{f_c} and $I_{\Delta f}$ evaluate the deviation between the band gap features f_c and Δf and the target features f_0 and Δf_0, respectively. These definitions are chosen so that the cost function is unitary ($0 < \mathscr{F} < 1$).

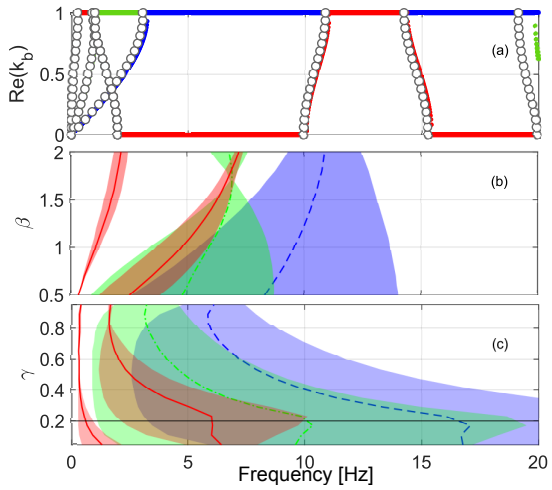


Figure 2. (Color online) Analysis of the dispersion relation of a bi-material PC pipe with $l_{tot} = 0.1$ m; (a) Real part of the dispersion relation with $\gamma = 0.2$, $R_1 = 8$ mm and $\beta = 0.5$ calculated by both the semi-analytical model (coloured dots, (•) longidutinal, (•) flexural and (•) torsional) and 3D full FEM simulation (open circles ○); (b-c) evolutions of the band gap widths (coloured patches) and mid frequencies (lines) for the three wave types (same colour legend as in (a)) as function of (b) β with $\gamma = 0.5$ and (c) γ with $\beta = 0.5$. $l_{tot} = 0.1$ m. The horizontal black line denotes the configuration leading to the dispersion graph in (a).

This optimisation procedure is applied to the solution of the semi-analytical eigenvalue problems described above with a target absolute band gap [3-6] kHz, which is a typical range of interest for injection applications in the context of automotive industry[43]. A detailed study of the optimisation is given as supplementary material and concludes that to ensure both accuracy and fast convergence, the best choice for the weighting coefficient of the cost function is $[\alpha_{f_c}, \alpha_{\Delta f}] = [5/6, 1/6]$. The optimal geometry of the 1D PC pipe obtained under these conditions and without considering material losses is $X = [87\text{ mm}, 0.44, 7.5\text{ mm}, 0.5]$. From the optimised geometry in the conservative case, the final complex dispersion relation of the PC pipe shown in Fig.3(a) is calculated considering the viscoelastic losses for both aluminium and nylon via the complex Young modulus $E_i^c = E_i(1 + \imath\eta_i)$ with $\eta_A =$ 1e-4 and $\eta_N =$ 4e-2. Each wave type displays band gaps where the real part of the wavenumber is low while imaginary part is high (see coloured patches in Fig.3(b)). In the target range of frequencies, band gaps are well overlapping, the obtained absolute band gap is [3.2-5.7] kHz (grey patch in Fig.3(a)), which is slightly narrower than the target, due to the losses.

In order to experimentally evaluate the vibration mitigation performances due to the absolute band gap of the infinite PC pipe, a finite pipe demonstrator with 6 unit cells is man-

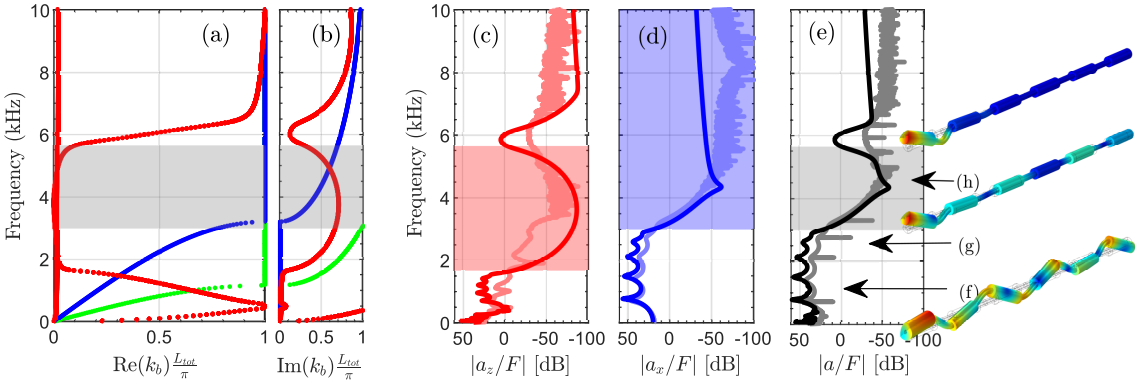


Figure 3. (Color online) Numerical analysis and experimental characterisation of the optimal PC pipe: (a) real part and (b) imaginary part of the optimised complex dispersion relation obtained by the Floquet-Bloch method and considering the viscoelastic losses (see main text). (•) longidutinal, (•) flexural and (•) torsional; measured (light line) and simulated (dark line) acceleration transfer functions in the (c) flexural, (d) longitudinal, (e) full loading cases; 3D views of the simulated total displacement in the full loading case at (f) 900 Hz where all wave types propagate, (g) 2500 Hz where only flexural band gap is opened and (h) 4500 Hz whithin the absolute band gap.

ufactured (Fig.1(a)). In the experimental set-up the demonstrator is suspended vertically from a rigid gallows mounted on an optical breadboard. A shaker (LDS V201) excites the demonstrator at its bottom end with a harmonic point force $\boldsymbol{F} = F_x.\boldsymbol{x} + F_y.\boldsymbol{y} + F_z.\boldsymbol{z}$ (see axis definition in Fig.1(e-f)) with a step-by-step sine in the range [0-10] kHz with a frequency step of 5Hz. 3 cases are considered : "flexural loading" such as $F_z \neq 0$ and $F_x = F_y = 0$ (the shaker is perpendicular to the pipe x-axis, only flexural waves are excited), "longitudinal loading" such as $F_x \neq 0$ and $F_y = F_z = 0$ (shaker aligned with the pipe x-axis, only longitudinal waves are excited), and "full loading" such as $F_{x,y,z} \neq 0$ as in Fig.1(d) where the force of the shaker is applied obliquely on a cut plane and off-centre with respect to the pipe x-axis so that all wave types are generated. The acceleration response $\boldsymbol{a} = a_x.\boldsymbol{x} + a_y.\boldsymbol{y} + a_z.\boldsymbol{z}$ is measured at the upper end by 2 three-axial accelerometers (PCB 356A01) that face each other (Fig.1(b)). This experimental situation is also numerically simulated from a full wave 3D FEM model in order to compare transfer functions.

Figure 3(c) represents both numerical and experimental transfer functions $|a_z/F|$ in the flexural loading case. The transfer functions show an attenuation of about 70dB in the frequency range corresponding to the predicted flexural band gap. The same trend is exhibited in Fig.3(d) which plots the transfer functions $|a_x/F|$ in the longitudinal loading case. Finally, the full loading case is shown in Fig.3(e) evidencing a strong attenuation in the transfer function $|a/F|$ in the range corresponding to the predicted absolute band gap. It is also worth noting that finite size effects can be seen at low frequencies with peaks of the transfer function corresponding to the Fabry-Pérot resonances of the system.

To complete the analysis, 3D views of the simulated total displacement field in the full loading case are shown in Fig.3(f-h). At 900Hz where all wave types propagate (Fig.3(f)), the superposition of all motions results in a complex total displacement field. At 2.5kHz (Fig.3(g)) the field mainly exhibits the longitudinal component, the flexural component being strongly attenuated due to band gap effect. At 4.5kHz (Fig.3(h)) the total field vanishes close to the excitation due to the total filtering effect associated to the absolute band gap.

To summarize, we apply the concept of absolute band gap to a bi-material PC pipe. Three 1D analytical Floquet-Bloch models giving the dispersion of both longitudinal, flexural and torsional waves considering losses are combined in an optimisation procedure to reach a unit cell design that exhibit absolute band gaps with target features. The hand-ability and reliability of such design methodology is shown through a set of cases detailed in the supplementary material, which brings a first main insight. On the top of that, the study of a 6-cells demonstrator shows both numerically and experimentally dips of the transfer functions corresponding to the absolute band gap analytically predicted, bringing a second main insight. These results illustrate how absolute band gaps in the high frequency domain can be applied to mitigate vibrations that may result in structure borne sound in some industrial systems. In further works, the design and optimisation of such PC pipes would be extended considering an enclosed pressurized liquid, hence considering couplings between acoustic and elastic waves.

SUPPLEMENTARY MATERIALS

The supplementary material details both the analytical wave dispersion models, the numerical optimization procedure and its application to a set of optimization cases.

ACKNOWLEDGMENTS

Authors thank Vitesco Technologies company and ANRT french agency who funded this research, Julien Nicolas and Stanislas Renard who manufactured the demonstrator, and Félix Foucard for his fruitfull contribution in the experiments.

DATA AVAILABILITY STATEMENT

The data that support the findings of this study are available from the corresponding author upon reasonable request.

REFERENCES

[1] M. Crocker, *Handbook of Noise and Vibration Control*, 3rd ed. (John Wiley Sons, New Jersey, New Jersey, 2007).

[2] L. Cremer, M. Heckl, and B. A. T. Petersson, *Structure-borne sound: structural vibrations and sound radiation at audio frequencies*, 3rd ed. (Springer, Berlin ; New York, 2005) oCLC: ocm57541302.

[3] P. Deymier, ed., *Acoustic Metamaterials and Phononic Crystals* (Springer, 2013).

[4] V. Romero-García and A.-C. Hladky-Hennion, eds., *Fundamentals and Applications of Acoustic Metamaterials: From Seismic to Radio Frequency* (Wiley-ISTE, 2019).

[5] J. D. Joannopoulus, S. G. Johnson, J. N. Winn, and R. D. Meade, *Photonic Crystals. Molding the Flow of Light* (Princeton University press, 2008).

[6] E. Economou and M. Sigalas, "Classical wave propagation in periodic structures: Cermet versus network topology," Phys. Rev. B **48 (18)**, 13434 (1993).

[7] M. Kushwaha, P. Halevi, L. Dobrzynski, and B. Djafari-Rouhani, "Acoustic band structure of periodic elastic composites," Phys. Rev. Lett. **71**, 2022–2025 (1993).

[8] L. Brillouin and M. Parodi, *Propagation des ondes dans les milieux périodiques* (Masson et Cie, 1956).

[9] R. Martínez-Sala, J. Sancho, J. V. Sánchez, V. Gómez, J. Llinares, and F. Meseguer, "Sound attenuation by sculpture," Nature **378**, 241 (1995).

[10] J. V. Sánchez-Pérez, D. Caballero, R. Martínez-Sala, C. Rubio, J. Sánchez-Dehesa, F. Meseguer, J. Llinares, and F. Gálvez, "Sound attenuation by a two-dimensional array of rigid cylinders," Phys. Rev. Lett. **80**, 5325–5328 (1998).

[11] M. Sigalas and E. Economou, "Elastic and acoustic wave band structure," J. Sound Vib. **158**, 377 (1992).

[12] A. Khelif, A. Choujaa, B. Djafari-Rouhani, M. Wilm, S. Ballandras, and V. Laude, "Trapping and guiding of acoustic waves by defect modes in a full-band-gap ultrasonic crystal," Phys. Rev. B **68**, 214301 (2003).

[13] A. Khelif, M. Wilm, V. Laude, S. Ballandras, and B. Djafari-Rouhani, "Guided elastic waves along a rod defect of a two-dimensional phononic crystal," Phys. Rev. E **69**, 067601 (2004).

[14] F. Cervera, L. Sanchis, J. V. Sánchez-Pérez, R. Martínez-Sala, C. Rubio, and F. Meseguer, "Refractive acoustic devices for airborne sound," Phys. Rev Lett. **88**, 023902–4 (2002).

[15] S.-C. Lin, T. Huang, J.-H. Sun, and T.-T. Wu, "Gradient-index phononic crystals," Phys. Rev. B **79** (2009).

[16] L. Feng, X. Liu, Y. Chen, Z. Huang, Y. Mao, Y. Chen, J. Zi, and Y. Zhu, "Negative refraction of acoustic waves in two-dimensional sonic crystals," Phys. Rev. B **72**, 033108 (2005).

[17] I. Pérez-Arjona, V. J. Sánchez-Morcillo, J. Redondo, V. Espinosa, and K. Staliunas, "Theoretical prediction of the nondiffractive propagation of sonic waves through periodic acoustic media," Phys. Rev. B **75**, 014304 (2007).

[18] A. Cebrecos, V. Romero-García, R. Picó, I. Pérez-Arjona, V. Espinosa, V. J. Sánchez-Morcillo, and K. Staliunas, "Formation of collimated sound beams by three-dimensional sonic crystals," Journal of Applied Physics **111**, 104910 (2012).

[19] V. Romero-García, J. Sánchez-Pérez, S. C. neira Ibáñez, and L. Garcia-Raffi, "Evidences of evanescent bloch waves in phononic crystals," Appl. Phys. Lett. **96**, 124102 (2010).

[20] A. Cebrecos, V. Romero-García, and J. P. Groby, "Complex dispersion relation recovery from 2d periodic resonant systems of finite size," Applied Sciences **9** (2019), 10.3390/app9030478.

[21] J. Sánchez-Pérez, C. Rubio, R. Martínez-Sala, R. Sánchez-Grandia, and V. Gómez, "Acoustic barriers based on periodic arrays of scatterers," Appl. Phys. Lett. **81**, 5240 (2002).

[22] V. Romero-García, J. V. Sánchez-Pérez, and L. M. Garcia-Raffi, "Tunable wideband bandstop acoustic filter based on two-dimensional multiphysical phenomena periodic systems." Jour. Appl. Phys. , 149041.

[23] T. Cavalieri, A. Cebrecos, J.-P. Groby, C. Chaufour, and V. Romero-García, "Three-dimensional multiresonant lossy sonic crystal for broadband acoustic attenuation: Application to train noise reduction," Applied Acoustics **146**, 1 – 8 (2019).

[24] H. Shen, J. Wen, D. Yu, and X. Wen, "The vibrational properties of a periodic composite pipe in 3d space," Journal of Sound and Vibration **328**, 57 – 70 (2009).

[25] Y. Zhang, D. Yu, and J. Wen, "Study on the band gaps of phononic crystal pipes with alternating materials in the radial and axial directions," Extreme Mechanics Letters **12**, 2 – 6 (2017), frontiers in Mechanical Metamaterials.

[26] J. O. Vasseur, P. A. Deymier, B. Djafari-Rouhani, Y. Pennec, and A.-C. Hladky-Hennion, "Absolute forbidden bands and waveguiding in two-dimensional phononic crystal plates," Phys. Rev.B **77**, 085415 (2008).

[27] A. Khelif, B. Aoubiza, S. Mohammadi, A. Adibi, and V. Laude, "Complete band gaps in two-dimensional phononic crystal slabs," Phys. Rev. E **74**, 046610 (2006).

[28] M. S. Kushwaha, P. Halevi, G. Martínez, L. Dobrzynski, and B. Djafari-Rouhani, "Theory of acoustic band structure of periodic elastic composites," Phys. Rev. B **49 (4)**, 2313–2322 (1994).

[29] J.-F. Robillard, O. B. Matar, J. O. Vasseur, P. A. Deymier, M. Stippinger, A.-C. Hladky-Hennion, Y. Pennec, and B. Djafari-Rouhani, "Tunable magnetoelastic phononic crystals," Applied Physics Letters **95**, 124104 (2009).

[30] O. R. Bilal and M. I. Hussein, "Ultrawide phononic band gap for combined in-plane and out-of-plane waves," Phys. Rev. E **84**, 065701 (2011).

[31] J. O. Vasseur, P. A. Deymier, G. Frantziskonis, G. Hong, B. Djafari-Rouhani, and L. Dobrzynski, "Experimental evidence for the existence of absolute acoustic band gaps in two-dimensional periodic composite media," Journal of Physics: Condensed Matter **10**, 6051–6064 (1998).

[32] H.-J. Zhao, H.-W. Guo, M.-X. Gao, R.-Q. Liu, and Z.-Q. Deng, "Vibration band gaps in double-vibrator pillared phononic crystal plate," Journal of Applied Physics **119**, 014903 (2016).

[33] K. Billon, M. Ouisse, E. Sadoulet-Reboul, M. Collet, P. Butaud, G. Chevallier, and A. Khelif, "Design and experimental validation of a temperature-driven adaptive phononic crystal slab," Smart Materials and Structures **28**, 035007 (2019).

[34] T. Delpero, S. Schoenwald, A. Zemp, and A. Bergamini, "Structural engineering of three-dimensional phononic crystals," Journal of Sound and Vibration **363**, 156 – 165 (2016).

[35] L. D'Alessandro, E. Belloni, R. Ardito, A. Corigliano, and F. Braghin, "Modeling and experimental verification of an ultra-wide bandgap in 3d phononic crystal," Applied Physics Letters **109**, 221907 (2016).

[36] O. R. Bilal, D. Ballagi, and C. Daraio, "Architected Lattices for Simultaneous Broadband Attenuation of Airborne Sound and Mechanical Vibrations in All Directions," Physical Review Applied **10**, 054060 (2018).

[37] G. Koo and Y. Park, "Vibration analysis of a 3-dimensional piping system conveying fluid by wave approach," International Journal of Pressure Vessels and Piping **67**, 249 – 256 (1996).

[38] K. F. Graff, *Wave motion in elastic solids* (Dover Publications, 1975).

[39] L. Liu and M. I. Hussein, "Wave Motion in Periodic Flexural Beams and Characterization of the Transition Between Bragg Scattering and Local Resonance," Journal of Applied Mechanics **79** (2011), 10.1115/1.4004592, 011003.

[40] A. Hvatov and S. Sorokin, "Free vibrations of finite periodic structures in pass- and stop-bands of the counterpart infinite waveguides," Journal of Sound and Vibration **347**, 200 – 217 (2015).

[41] A. Pelat, T. Gallot, and F. Gautier, "On the control of the first bragg band gap in periodic continuously corrugated beam for flexural vibration," Journal of Sound and Vibration **446**, 249 – 262 (2019).

[42] J. C. Lagarias, J. A. Reeds, M. H. Wright, and P. E. Wright, "Convergence properties of the nelder–mead simplex method in low dimensions," SIAM Journal on Optimization **9**, 112–147 (1998).

[43] T. Bourdon, R. Weber, and J. Massinger, "Virtual nvh prototyping of fuel components design - focus on high pressure pumps and scr injectors," in *SAE Technical Paper* (SAE International, 2017).